Confirmation and Characterization of the Eccentric, Warm Jupiter TIC 393818343 b with a Network of Citizen Scientists

Lauren A. Sgro[1], Paul A. Dalba[1,2,24], Thomas M. Esposito[1,3,4], Franck Marchis[1,3], Diana Dragomir[5],
Steven Villanueva, Jr.[6,25], Benjamin Fulton[7], Mario Billiani[8], Margaret Loose[9], Nicola Meneghelli[10],
Darren Rivett[11], Fadi Saibi[12], Sophie Saibi[12], Bryan Martin[13], Georgios Lekkas[14], Daniel Zaharevitz[15],
Robert T. Zellem[16,14], Ivan A. Terentev[17], Robert Gagliano[18], Thomas Lee Jacobs[19], Martti H. Kristiansen[20],
Daryll M. LaCourse[21], Mark Omohundro[22], and Hans M. Schwengeler[23]

[1] SETI Institute, Carl Sagan Center, 339 Bernardo Ave., Suite 200, Mountain View, CA 94043, USA; lsgro@seti.org
[2] Department of Astronomy and Astrophysics, University of California, Santa Cruz, CA 95064, USA
[3] Unistellar, 5 allée Marcel Leclerc, bâtiment B, Marseille, 13008, France
[4] Department of Astronomy, University of California, Berkeley, CA 94720, USA
[5] Department of Physics & Astronomy, University of New Mexico, 1919 Lomas Blvd. NE, Albuquerque, NM 87131, USA
[6] NASA Goddard Space Flight Center, 8800 Greenbelt Rd., Greenbelt, MD 20771, USA
[7] NASA Exoplanet Science Institute/Caltech-IPAC, MC 314-6, 1200 E. California Blvd., Pasadena, CA 91125, USA
[8] Unistellar Network, Vienna, Austria[26]
[9] Unistellar Network, Santa Fe, NM, USA[26]
[10] Unistellar Network, Zevio, Verona, Italy[26]
[11] Unistellar Network, Lake Macquarie, NSW, Australia[26]
[12] Unistellar Network, Sunnyvale, CA, USA[26]
[13] Exoplanet Watch, Great Falls, MT, USA[26]
[14] Exoplanet Watch, Thessaloniki, Greece[26]
[15] Exoplanet Watch, Frederick, MD, USA[26]
[16] Jet Propulsion Laboratory, California Institute of Technology, 4800 Oak Grove Dr., Pasadena, CA 91109, USA
[17] Visual Survey Group, Petrozavodsk, Russia[26]
[18] Visual Survey Group, Glendale, AZ, USA[26]
[19] Visual Survey Group, Bellevue, WA, USA[26]
[20] Brorfelde Observatory, Observator Gyldenkernes Vej 7, DK-4340 Tølløse, Denmark
[21] Visual Survey Group, Marysville, WA, USA[26]
[22] Department of Physics, University of Oxford, Denys Wilkinson Building, Keble Rd., Oxford, OX13RH, UK[26]
[23] Visual Survey Group, Bottmingen, Switzerland

Abstract

NASA's Transiting Exoplanet Survey Satellite (TESS) has identified over 7000 candidate exoplanets via the transit method, with gas giants among the most readily detected due to their large radii. Even so, long intervals between TESS observations for much of the sky lead to candidates for which only a single transit is detected in one TESS sector, leaving those candidate exoplanets with unconstrained orbital periods. Here, we confirm the planetary nature of TIC 393818343 b, originally identified via a single TESS transit, using radial velocity data and ground-based photometric observations from citizen scientists with the Unistellar Network and Exoplanet Watch. We determine a period of $P = 16.24921\ ^{+0.00010}_{-0.00011}$ days, a mass $M_P = 4.34 \pm 0.15\ M_{\rm J}$, and semimajor axis $a = 0.1291\ ^{+0.0021}_{-0.0022}$ au, placing TIC 393818343 b in the "warm Jupiter" population of exoplanets. With an eccentricity $e = 0.6058 \pm 0.0023$, TIC 393818343 b is the most eccentric warm Jupiter to be discovered by TESS orbiting less than 0.15 au from its host star and therefore an excellent candidate for follow-up, as it may inform our future understanding of how hot and warm Jupiter populations are linked.

1. Introduction

In 2023 September, the NASA Exoplanet Archive (NEA) announced the 5500th confirmed exoplanet.[27] This growing number is far from the first exoplanet discovery of 51 Peg b (Mayor & Queloz 1995), which we now know as a hot Jupiter. Hot Jupiters are typically categorized as having $\geqslant 0.25\ M_{\rm J}$ and orbital periods of $\leqslant 10$ days and are among the most easily detected via the transit method due to their large radii, small semimajor axes, and frequent transits. However, a growing population of discovered warm Jupiters ($P \approx 10$–200 days, $a = 0.1$–0.5 au) has informed our understanding of hot Jupiter formation as it is expected that hot Jupiters reach their orbits via migration from outside the snow line (Dawson & Johnson 2018). Migration pathways are favored over in situ formation in part due to the large amount of solids required, $\sim 10\ M_{\rm E}$, for core accretion (Rafikov 2006) and the lack of observational evidence for formation by gravitational instability although there is active work investigating this latter

---

Table 1
Summary of Photometric Observations

UTC Date	Transit Epoch	Observer	Telescope	Filter
2022 Aug 19	0	…	TESS	TESS
2023 May 23	17	N. Meneghelli	eVscope-A	Clear
2023 May 23	17	M. Billiani	eVscope-B	Clear
2023 Jun 24	19	B. Martin	12 inch Dall–Kirkham	I
2023 Jun 24	19	D. Rivett	eVscope-C	Clear
2023 Jun 24	19	F. & S. Saibi	eVscope-D	Clear
2023 Jun 24	19	M. Loose	eVscope-E	Clear

scenario (Hall et al. 2020; Paneque-Carreño et al. 2021). Therefore, this intermediate population of warm Jupiters may be progenitors of hot Jupiters and links to our solar system's distant, cold Jupiter.

Two primary migration pathways have been proposed that may produce hot Jupiters: disk migration, in which an exchange of angular momentum with the surrounding protoplanetary disk causes the planet's migration (Goldreich & Tremaine 1980; Baruteau et al. 2014), and high-eccentricity (tidal) migration, where a gas giant on an eccentric orbit undergoes tidal dissipation due to close periastron passage with the host star, reducing the planet's semimajor axis and therefore circularizing the orbit (Rasio & Ford 1996; Wu & Murray 2003, see Dawson & Johnson 2018 for a recent review). To experience tidal migration, a warm Jupiter must have a particular combination of eccentricity and semimajor axis that brings it sufficiently close to its host. Multiple mechanisms for the origin of this high eccentricity have been proposed, e.g., Kozai-Lidov oscillations (Kozai 1962; Lidov 1962; Naoz 2016), secular interactions (Wu & Lithwick 2011; Petrovich & Tremaine 2016), and planet–planet scattering (Rasio & Ford 1996; Ford & Rasio 2006; Chatterjee et al. 2008; Nagasawa et al. 2008). However, only three warm Jupiters are known that exhibit an eccentricity large enough to eventually join the hot Jupiter population via tidal migration, implying an entire population of hot Jupiters with only suspected origins (Naef et al. 2001; Dong et al. 2021; Gupta et al. 2024). The population of eccentric warm Jupiters with unknown fates is important to study and add to as their evolution history may contain an important piece of the planetary formation puzzle.

With the conclusion of the Kepler and K2 missions, NASA's Transiting Exoplanet Survey Satellite (TESS; Ricker et al. 2015) has become the most promising observatory with which to detect warm gas giants. There are already 27 confirmed planets in the NEA (NASA Exoplanet Archive 2024)[28] representative of this population ($a = 0.1$–0.5 au, $M \geqslant 0.25$ M_J, and P ranging from 10 to 98 days), all discovered by TESS despite its recent launch in 2018. However, TESS only observes each sector of the sky for an average of 27.4 days, leaving a population of TESS candidates for which only a single transit has been detected. Such candidates have poorly constrained periods and must rely on follow-up photometric and radial velocity (RV) efforts to confirm system properties. One such way to detect subsequent transits is via photometry gathered from the citizen science community. Enlisting such global networks mitigates the limitations faced by professional telescope facilities, such as visibility and weather restrictions of a single location and finite available time. The exoplanet community is already successfully working with these networks through programs such as the Unistellar Network (Peluso et al. 2023), Exoplanet Watch (Zellem et al. 2020), and ExoClock (Kokori et al. 2022, 2023). Here we add to the quickly growing list of citizen science successes in exoplanet follow-up.

We present the confirmation of a high-eccentricity ($e = 0.6058 \pm 0.0023$) warm Jupiter TIC 393818343 b with $P = 16.24921^{+0.00010}_{-0.00011}$ days using both ground-based transit and RV data. We first identified a single transit signature via visual inspection in Sector 55 TESS data as part of the Visual Survey Group (VSG; Kristiansen et al. 2022). Follow-up observations and analyses with Lick Observatory, the Unistellar Network of Citizen Astronomers, and Exoplanet Watch confirm the existence of this exoplanet. We present our findings in the following order: in Section 2 we present our observations of TIC 393818343 b, in Section 3 we detail our methods of modeling the system in order to plan photometric observations and confirm the planet, in Section 4 we discuss our results, and in Section 5 we discuss the implications of this discovery and potential future observations. Finally, in Section 6 we give an overview of our findings.

2. Observations

2.1. TESS Photometry

TIC 393818343 was observed by TESS at a 2 minute cadence during its extended mission in Sector 55 from 2022 August 5 to September 1. We use the image data as processed by the Science Processing Operations Center (Jenkins et al. 2016) at NASA Ames Research Center (MAST Team 2021). Although no evidence of two or more transits was found by the Quick-Look Pipeline, additional analyses were carried out by the VSG. Using the `LcTools` software package (Schmitt et al. 2019; Schmitt & Vanderburg 2021), this group of professional and citizen scientists detected a single transit in TESS data taken on 2022 August 19, prompting a Doppler monitoring follow-up campaign. We refer to the candidate exoplanet that caused this transit signature as TIC 393818343.01. The TESS observation, along with all other photometric observations used in this work, are detailed in Table 1. The candidate TIC 393818343.01 was further categorized as a TESS object of interest, TOI 6883.01, on 2024 February 1 (Conzo & Moriconi 2024).

2.2. High Resolution Echelle Spectrometer and Levy Spectroscopy

After the discovery of the Sector 55 TESS transit by the VSG, we obtained a high signal-to-noise (S/N > 200) template spectrum of TIC 393818343 taken with the High Resolution

---
[28] Accessed on 2024 May 22 at 20:00 UTC.

Echelle Spectrometer (HIRES; Vogt et al. 1994) at W. M. Keck Observatory without the HIRES iodine cell. We analyzed this spectrum using the synthetic spectral matching tool Spec-Match (Petigura et al. 2017) to gather basic stellar parameters as priors in our global system modeling including effective temperature $T_{\rm eff}$, surface gravity log$g$, metallicity [Fe/H], and projected rotational velocity $v$sin$i$. After confirming via the HIRES data that TIC 393818343 was an appropriate target for Doppler spectroscopy, we proceeded with a follow-up campaign.

From 2022 October to 2023 July, we initiated a Doppler monitoring campaign of TIC 393818343 using the Levy Spectrograph on the Automated Planet Finder (APF) Telescope at Lick Observatory in Mt. Hamilton, California (Radovan et al. 2014; Vogt et al. 2014). The Levy Spectrograph is a high-resolution slit-fed optical echelle spectrometer with $R \approx 114{,}000$ (Radovan et al. 2010) and an iodine cell for precise wavelength calibration (Butler et al. 1996). Over this observing period, we gathered 56 RV measurements with uncertainties ranging from 3.6 to 7.8 ms^{-1}. For each spectrum, we deduced RV using a forward-modeling procedure (Butler et al. 1996; Fulton et al. 2015) in which we used the Keck-HIRES spectrum as a template. Obtaining a template spectrum of the necessary quality was more efficient with Keck-HIRES due to the aperture, which is 10 m as opposed to APF's 2.4 m aperture. All RV measurements from APF-Levy are presented in Table 2, and time series RVs are shown in Figure 1.

We combined these RV measurements with the TESS photometry using EXOFASTv2 (Eastman et al. 2013, 2019) to predict future transit windows, which enabled a ground-based photometric campaign for TIC 393818343.01 transits. The follow-up photometry is described in Sections 2.3 and 2.4, while system modeling is described in Section 3.

2.3. Unistellar Network Observations

Using the Unistellar Network of citizen scientists, we obtained photometry of TIC 393818343 in accordance with our predicted transit windows calculated as described in Section 3. This network consists of observers around the world who operate mobile 114 mm Newtonian imaging telescopes, called eVscopes, produced by Unistellar (Marchis et al. 2020). The two models of eVscope both utilize a SONY CMOS image sensor, either model IMX224 or IMX347, with a $28' \times 37'$ or $34' \times 47'$ field of view (FOV), respectively. See Peluso et al. (2023) for an in-depth review of the Unistellar Network Exoplanet program.

On 2023 May 23, two citizen scientists observed TIC 393818343 during a predicted transit window from Austria and Italy. This prompted another follow-up campaign (see Section 3) on 2023 June 24 that included three participating Unistellar Network telescopes located in California, USA, and Australia.

For each eVscope observation, which varied in duration, off-target or saturated frames were removed from the data set. All other images were dark subtracted and plate solved. Calibrated frames were then aligned and averaged together up to a total integration time of 2 minutes each to increase the star S/N and reduce computation time in subsequent steps. Following the procedure of Dalba & Muirhead (2016) and Dalba et al. (2017), differential photometry was performed on each data set using an optimized combination of up to ten reference stars. The pool of potential reference stars is created by identifying all stars in

Table 2
RV Measurements of TIC 393818343 from APF-Levy

BJD$_{\rm TDB}$	RV (m s^{-1})
2459858.773894	679.6 ± 4.0
2459861.776856	6.4 ± 4.3
2459864.782496	-110.4 ± 4.4
2459868.654536	-128.9 ± 3.9
2459872.684238	48.9 ± 5.8
2459897.626448	-128.3 ± 3.9
2459904.706206	4.5 ± 3.8
2460044.993459	-127.8 ± 3.7
2460050.016955	-53.0 ± 3.6
2460055.956763	84.3 ± 4.3
2460060.938359	-143.0 ± 4.1
2460061.929630	-126.5 ± 4.6
2460062.935416	-123.3 ± 4.5
2460063.943645	-124.6 ± 4.0
2460064.929811	-90.1 ± 6.0
2460072.904212	10.6 ± 6.5
2460073.922257	-59.6 ± 4.5
2460074.940567	-99.8 ± 7.8
2460075.891244	-114.0 ± 4.1
2460076.895873	-135.5 ± 4.5
2460078.891853	-126.6 ± 3.7
2460081.896280	-77.8 ± 4.4
2460083.911727	37.0 ± 3.6
2460084.875597	211.9 ± 4.6
2460085.866808	534.0 ± 4.0
2460087.860502	193.1 ± 3.6
2460088.945967	11.3 ± 3.9
2460089.862875	-59.5 ± 4.2
2460091.854226	-121.5 ± 4.9
2460093.968028	-138.0 ± 6.5
2460095.840985	-142.0 ± 6.8
2460096.851126	-102.3 ± 4.5
2460097.835640	-89.7 ± 4.8
2460098.891130	-53.1 ± 3.9
2460104.828737	55.1 ± 4.1
2460105.964703	-41.2 ± 5.0
2460106.848495	-69.4 ± 7.7
2460107.823347	-98.4 ± 7.2
2460108.871167	-123.8 ± 3.8
2460109.810574	-126.8 ± 4.7
2460110.805436	-128.9 ± 4.8
2460111.796328	-119.6 ± 5.9
2460112.950157	-107.5 ± 4.0
2460113.824174	-89.9 ± 5.0
2460115.789096	3.5 ± 5.6
2460118.864396	704.4 ± 4.2
2460119.859491	321.7 ± 4.4
2460121.786157	-11.4 ± 4.2
2460123.811574	-115.6 ± 4.1
2460125.961876	-130.1 ± 3.7
2460128.882675	-112.7 ± 4.3
2460131.882008	-22.3 ± 3.7
2460133.902699	272.0 ± 5.0
2460135.963745	382.6 ± 4.2
2460138.837038	-49.3 ± 4.2
2460140.992830	-118.3 ± 3.8

each image (other than the target), measuring their fluxes, and removing those which are saturated or do not appear in $\geqslant 50\%$ of the frames. We then select up to ten of the brightest stars and generate individual reference light curves for each of them. Next, we generate "composite reference star" light curves from
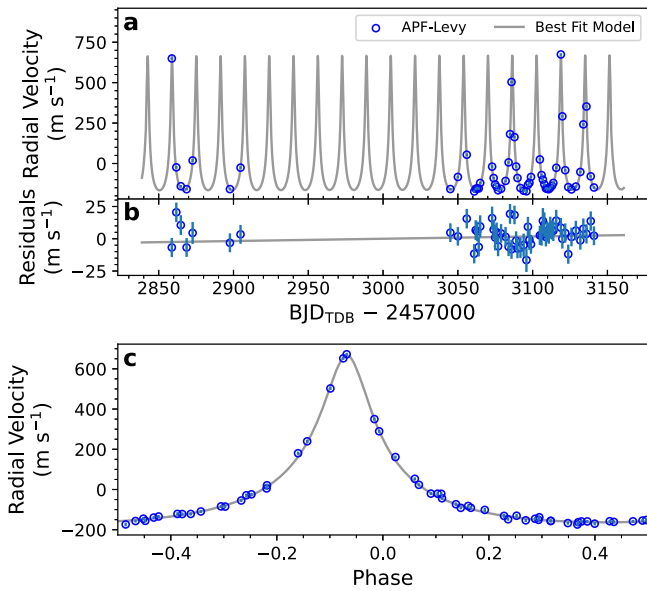
Figure 1. APF-Levy RVs of TIC 393818343. Panel (a) is the time series. Panel (c) is phase-folded on the best-fit ephemeris. Panel (b) shows that an additional long-term RV trend may be present although from this data set alone it is statistically consistent with no trend.

every unique combination of those individual reference light curves, where the combination is a median across stars (not time). As a result, we produce up to 1023 composite reference star light curves with which to normalize the target star's flux. The best normalized target light curve from that group is selected as the one with the smallest residuals in the out-of-transit measurements when compared to a flat model. An optimal aperture size is deduced for each observation by fitting a 2D Gaussian function to the target across all images in the data set and calculating a weighted average standard deviation across all frames, where the weights are inversely proportional to the variance. For the only Unistellar data set crossing ingress, we tested a variety of aperture sizes from $14''$ to $24''$ to ensure that the ingress signal was not introduced by a varying PSF as seeing conditions changed. With this additional analysis, we confirmed that the ingress signal was present in all iterations of the photometry and that therefore our detection was robust. We do not detrend for air mass for any of the four data sets that contain in-transit data since they do not have both pre- and post-transit data points.

We note that there is a spatially coincident, unbound star, Gaia Data Release 3 (DR3) 4233021429372256512, seen $6''5$ from TIC 393818343 that can appear blended with the target in ground-based images. We include this nearby source in the target aperture when performing differential photometry and discuss its potential impact in Section 4.

2.4. Exoplanet Watch Observations

Several citizen scientists associated with Exoplanet Watch observed during both campaigns with telescopes other than eVscopes. Two observations on 2023 May 23 were taken outside of the transit window and therefore contained only baseline data. We do not include these observations in Table 1 or in subsequent modeling. However, a 4.5 hr observation taken 2024 June 24 from Utah, USA, did cover the predicted transit window and is detailed in Table 1. The observer used a Johnson I filter on a 305 mm Dall–Kirkham telescope equipped

with a ZWO ASI 294mm CMOS camera (FOV $63' \times 31'$) and an exposure time of 90 s per image. The data were 2×2 binned and calibrated with dark, flat, and bias frames using EXOTIC (Zellem et al. 2020). EXOTIC was also used by the observer to perform plate solving and differential photometry with a $19''5$ diameter target aperture.

3. Methods

In this section we describe the initial system modeling, the two follow-up photometric campaigns, and the subsequent modeling once additional data were received.

3.1. Initial System Modeling

Using the single TESS transit and the subsequent APF-Levy RV observations, we initially modeled the stellar and planetary parameters for the TIC 393818343 system via the EXOFASTv2 suite (Eastman et al. 2013, 2019), which jointly considers photometry and RV data when modeling a system. Preliminary modeling included TESS photometry and APF-Levy RV data through May of 2023 along with archival broadband photometry from Gaia Data Release 2 (Gaia Collaboration et al. 2016, 2018), the Two Micron All Sky Survey (Cutri et al. 2003), and the Wide-field Infrared Survey Explorer (Cutri et al. 2014). These archival data sets, as well as Gaia parallax measurements, were used by EXOFASTv2 to fit spectral energy distributions (SEDs) from MIST stellar evolutionary models (Dotter 2016) to gather host-star properties.

Based on the Specmatch analysis of the HIRES TIC 393818343 template spectrum, we placed normal host-star priors on $T_{\rm eff}$ and [Fe/H], as well as on parallax using the Gaia DR3 parallax data corrected for the zero-point offset (Vallenari et al. 2023; Lindegren et al. 2021). We also placed a uniform prior on extinction in the V band ($A_V \leqslant 0.2455$) derived from Galactic dust maps (Schlafly & Finkbeiner 2011). These informative priors are listed at the top of Table 3, and noninformative priors used by EXOFASTv2 can be found in Table 3 of Eastman et al. (2019).

We consider the fit—including archival, TESS, and RV data—converged in accordance with the default EXOFASTv2 statistics, where the number of independent draws of the underlying posterior probability distribution is $T_z > 1000$ (Ford & Rasio 2006) and the Gelman–Rubin statistic (Gelman & Rubin 1992) < 1.01 for every fitted parameter. This EXOFASTv2 analysis initially returned a posterior period with 68% confidence of 16.2511 ± 0.0046 days and duration of 4.2 hr, predicting the next mid-transit time to be $T_o = 2460087.50889 \pm 0.08$ BJD$_{\rm TDB}$, or UTC 2023 May 23 00:09:19.

3.2. Initial Photometric Campaign and Subsequent Modeling

We refer to this particular transit window with mid-transit time $T_o = 2460087.50889 \pm 0.08$ BJD$_{\rm TDB}$ as Epoch 17, where Epoch 0 is defined as the TESS Sector 55 transit. We prompted the Unistellar Network and Exoplanet Watch to observe this 2σ window plus half the transit time, a 12 hr span during which we obtained four multi-hour observations. Two of these observations consisted only of baseline data; thus, they are not included in our tables or figures (see Section 2.4).

Two of the Epoch 17 observations from the Unistellar Network spanned the projected egress time. For each light curve, we use a custom transit fitting routine adapted for

Table 3
Median Values and 68% Confidence Interval for the TIC 393818343 System

Parameter	Units	Values		
Informative Priors:				
$T_{\rm eff}$	Effective Temperature (K)	$\mathcal{N}(5800, 100)$		
[Fe/H]	Metallicity (dex)	$\mathcal{N}(0.32, 0.06)$		
ϖ	Parallax (mas)	$\mathcal{N}(10.644, 0.397)$		
A_V	V-band Extinction (mag)	$\mathcal{U}(0, 0.2455)$		
Stellar Parameters:				
M_*	Mass ($M_\odot$)	$1.082^{+0.055}_{-0.056}$		
R_*	Radius ($R_\odot$)	1.086 ± 0.020		
L_*	Luminosity ($L_\odot$)	$1.168^{+0.065}_{-0.063}$		
$F_{\rm Bol}$	Bolometric Flux (cgs)	$0.00000000423 \pm 0.00000000023$		
ρ_*	Density (cgs)	$1.198^{+0.040}_{-0.058}$		
$\log g$	Surface gravity (cgs)	$4.402^{+0.013}_{-0.018}$		
$T_{\rm eff}$	Effective Temperature (K)	5756^{+67}_{-66}		
[Fe/H]	Metallicity(dex)	0.318 ± 0.058		
$[{\rm Fe/H}]_0$	Initial Metallicity[a]	0.299 ± 0.057		
Age	Age (Gyr)	$3.8^{+2.6}_{-2.1}$		
EEP	Equal Evolutionary Phase[b]	355^{+33}_{-22}		
A_V	V-band extinction (mag)	$0.127^{+0.073}_{-0.076}$		
$\sigma_{\rm SED}$	SED photometry error scaling	$1.28^{+0.49}_{-0.30}$		
ϖ	Parallax (mas)	10.643 ± 0.039		
d	Distance (pc)	$93.96^{+0.35}_{-0.34}$		
$\dot{\gamma}$	RV slope[c] (m/s/day)	0.001 ± 0.015		
Planetary Parameters:		b		
P	Period (days)	$16.24921^{+0.00010}_{-0.00011}$		
R_P	Radius ($R_{\rm J}$)	$1.087^{+0.023}_{-0.021}$		
M_P	Mass ($M_{\rm J}$)	4.34 ± 0.15		
T_C	Time of conjunction ($\rm BJD_{TDB}$)	$2459811.24020^{+0.00025}_{-0.00024}$		
a	Semimajor axis (AU)	$0.1291^{+0.0021}_{-0.0022}$		
i	Inclination (Degrees)	$89.57^{+0.30}_{-0.38}$		
e	Eccentricity	0.6058 ± 0.0023		
ω_*	Argument of Periastron (Degrees)	1.69 ± 0.49		
T_{eq}	Equilibrium temperature[d] (K)	$805.5^{+9.6}_{-9.4}$		
$\tau_{\rm circ}$	Tidal circularization timescale (Gyr)	$26.2^{+2.1}_{-2.6}$		
K	RV semi-amplitude (m/s)	414.8 ± 2.8		
R_P/R_*	Radius of planet in stellar radii	$0.10295^{+0.00065}_{-0.00062}$		
a/R_*	Semimajor axis in stellar radii	$25.60^{+0.28}_{-0.42}$		
δ	$(R_P/R_*)^2$	0.01060 ± 0.00013		
$\delta_{\rm I}$	Transit depth in I (fraction)	$0.01237^{+0.00038}_{-0.00037}$		
$\delta_{\rm Clear}$	Transit depth in Clear (fraction)	0.01205 ± 0.00025		
$\delta_{\rm TESS}$	Transit depth in TESS (fraction)	0.01270 ± 0.00022		
τ	Ingress/egress transit duration (days)	$0.01634^{+0.00067}_{-0.00024}$		
T_{14}	Total transit duration (days)	$0.17294^{+0.00089}_{-0.00082}$		
b	Transit impact parameter	$0.119^{+0.10}_{-0.083}$		
b_S	Eclipse impact parameter	$0.123^{+0.11}_{-0.086}$		
τ_S	Ingress/egress eclipse duration (days)	$0.01698^{+0.00069}_{-0.00033}$		
$T_{S,14}$	Total eclipse duration (days)	0.1791 ± 0.0020		
ρ_P	Density (cgs)	$4.22^{+0.16}_{-0.24}$		
$\log g_P$	Surface gravity	$3.962^{+0.010}_{-0.018}$		
Θ	Safronov Number	$0.952^{+0.019}_{-0.020}$		
$\langle F \rangle$	Incident Flux (10^9 erg s^{-1} cm^{-2})	$0.0682^{+0.0033}_{-0.0031}$		
T_P	Time of Periastron ($\rm BJD_{TDB}$)	$2459810.145^{+0.015}_{-0.016}$		
T_S	Time of eclipse ($\rm BJD_{TDB}$)	2459808.973 ± 0.019		
$e \cos \omega_*$	…	0.6055 ± 0.0023		
$e \sin \omega_*$	…	0.0179 ± 0.0052		
Wavelength Parameters:		Dall–Kirkham (I)	eVscope (Clear)	TESS
u_1	linear limb-darkening coeff	0.294 ± 0.050	0.425 ± 0.026	0.339 ± 0.033
u_2	quadratic limb-darkening coeff	0.269 ± 0.050	0.271 ± 0.024	0.273 ± 0.046

Parameter	Units	Values
Telescope Parameters:		APF-Levy
$\gamma_{\rm rel}$	Relative RV Offset[c] (m/s)	33.1 ± 1.5
σ_J	RV Jitter (m/s)	$7.23^{+1.1}_{-0.97}$

Notes. See Table 3 in Eastman et al. (2019) for a detailed description of all parameters and default, noninformative priors. Informative priors listed as $\mathcal{N}(a, b)$ indicates a normal distribution with mean a and standard deviation b, while $\mathcal{U}(a, b)$ indicates a uniform distribution over the interval $[a, b]$.
[a] The metallicity of the star at birth.
[b] Corresponds to static points in a star's evolutionary history. See Section 2 in Dotter (2016).
[c] Reference epoch = 2459999.883362.
[d] Assumes no albedo and perfect redistribution.

eVscope data that uses the `pycheops` Python package and a least-squares minimization to model the transit (Peluso et al. 2023). Due to the partial nature of the individual light curves, the transit duration and period were fixed to those values determined by `EXOFASTv2`, while the mid-transit time and depth were allowed to vary within 2σ and 40% of the expected value, respectively. Our custom routine then uses the Schwarz criterion rankings from Kass & Raftery (1995) to determine if the fitted transit is statistically favored over a flat line, among other tests that ensure the model is reasonable. As a result of the analyses included in this routine, observation during Epoch 17 resulted in a preliminary detection of egress.

The two Epoch 17 data sets containing egress signatures were then combined into the `EXOFASTv2` fit with the previous TESS photometry and continued RV monitoring data through 2023 June in order to refine the period to $P = 16.24927 \pm 0.0046$ days.

3.3. Confirmation Photometric Campaign

We initiated a confirmation campaign to observe a predicted transit with mid-transit time at $T_o = 2460119.97632 \pm 0.08$ BJD$_{\rm TDB}$, or 2023 June 24 11:18:53 UTC, two periods after our initial endeavor. We refer to this transit window, which spanned 8 hr to allow for 2 hr baseline observations in addition to the expected transit duration of ~ 4 hr, as Epoch 19.

Four observers took part in our Epoch 19 confirmation campaign, with their data covering predicted ingress and egress. Light curves from all photometric campaign epochs are presented individually in Figure 2. The Epoch 19 campaign was successful, as the transit was detected in a joint light curve combining the three Unistellar eVscope data sets, shown in Figure 3. Another observation from Exoplanet Watch also detected ingress independently. These four data sets were then combined with the complete APF RV data set once Doppler monitoring concluded in 2023 July, as well as with the ground-based Epoch 17, TESS Epoch 0, and archival photometry, to be used as input for a final `EXOFASTv2` analysis following the process described in Section 3.1. We discuss the results of this analysis in Section 4.

4. Results

From the best-fit `EXOFASTv2` solution using all of the available data outlined in Section 3.3, we confirm that TIC 393818343.01, hereafter TIC 393818343 b, is a giant planet with an eccentric orbit at $e = 0.6058 \pm 0.0023$. The best-fit period $P = 16.24921^{+0.00010}_{-0.00011}$, in close agreement with the initial estimates, and best-fit mass and radius of $M_P = 4.34 \pm 0.15\ M_J$ and $R_P = 1.087^{+0.023}_{-0.021}\ R_J$, respectively,
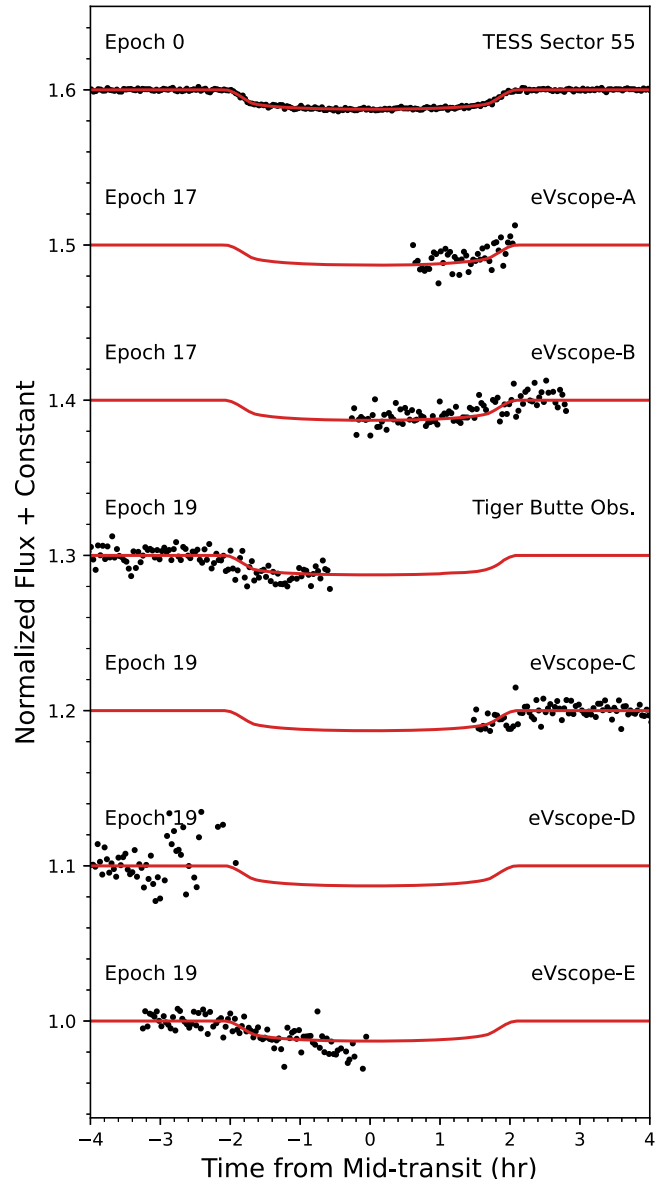

Figure 2. Individual transit observations of TIC 393818343 b and the best-fit model from `EXOFASTv2` shown in red. The names of observers and relevant epochs are listed in Table 1.

place this planet in the warm Jupiter category of gas giants. Posteriors of the `EXOFASTv2` modeling are listed in Table 3.

There is a foreground star, Gaia DR3 4233021429372256512, at a distance of 84.5 pc compared to the target's distance of
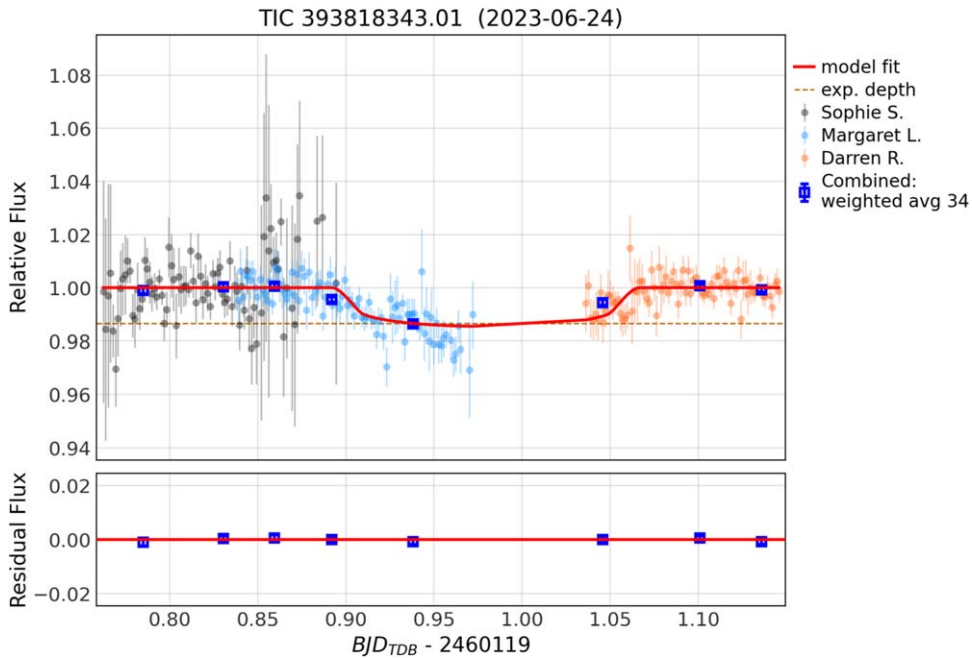
Figure 3. Light curve of observations taken by Unistellar Network observers during the second photometric confirmation campaign (Epoch 19, described in Section 3.3). Note that observer Margaret L.'s data were affected by fog near the expected mid-transit time.

93.5 pc (Bailer-Jones et al. 2018), with which the target is blended in ground-based images. We included this star in the target aperture when performing differential photometry, running the risk that the transit depth could be diluted when compared to TESS observations, which are corrected for this dilution, due to the excess baseline flux from the companion. However, we found that the modeled transit depth in Clear, the filter representative of the eVscope, is in agreement with the transit depth measured from the TESS light curve (see Table 3).

To test this agreement between the corrected TESS and the ground-based data, we assume that the depth of the measured TESS transit is 1.27% of the host-star flux. Note that we used the lightkurve package (Lightkurve Collaboration et al. 2018) as described in Peluso et al. (2024) to reproduce the TESS light curve discovered by the VSG and deduce the transit depth, which uses the TESS PDCSAP flux that has already been corrected for crowding. The crowding metric from the TESS TargetPixelFile for the Sector 55 observation, or CROWDSAP, is 0.77034879, indicating that approximately 23% of flux in the TESS aperture is from objects other than the host star. If we consider this additional flux in our depth calculation, the resultant "diluted" depth is 1.03%. This depth is only 0.24% from the corrected transit depth, which is well within the noise floor of the eVscope observations. We obtain a similar result when considering the "diluted" depth in relation to the difference in magnitude between the host and foreground star (1.38 mag, or 28% of the host-star magnitude in Gaia $G_{\rm rp}$). Therefore, we ignore the effects of dilution from Gaia DR3 4233021429372256512 in our modeling using ground-based data.

Additionally, the foreground star is identified as a variable in the Gaia DR3 catalog via the phot_variable_flag; however, it is unreasonable that the star could cause the observed transit. Gaia DR3 4233021429372256512 is a 10.31 magnitude star in the Gaia $G_{\rm RP}$ band, while TIC 393818343 $G_{\rm RP} = 8.93$ (the TESS bandpass is centered on the traditional Cousins I band at 786.5 nm, while $G_{\rm RP}$ is centered at 797 nm).

Although the Gaia data indicate a range in $G_{\rm RP}$ of 0.0163 for the foreground star, the duration of the variability is listed as time_duration_rp = 928.9 days. As this value is over 5000 times the transit duration, it is unlikely that the variability of the foreground star is responsible for the photometric transit signature that was observed and predicted via the EXOFASTv2 analysis.

5. Discussion

5.1. Eccentricity and Tidal Circularization

With an eccentricity $e = 0.6058 \pm 0.0023$, TIC 393818343 b occupies a sparsely populated orbital parameter space. This feature is evident in Figure 4, which compares e and a for a subset of confirmed planets with mass measurements from the NEA (NASA Exoplanet Archive 2024).[29] The most eccentric known exoplanets include HD 80606 b ($e = 0.93$; Naef et al. 2001), TOI-3362 b ($e = 0.81$; Dong et al. 2021), and another warm Jupiter with $e = 0.93$ (Gupta et al. 2024), all of which are expected to tidally circularize before their host star evolves off the main sequence. To compare, we calculate via EXOFASTv2 the tidal circularization timescale, $\tau_{\rm circ}$, to be $26.2^{+2.1}_{-2.6}$ Gyr (see Equation (3) from Adams & Laughlin 2006, assuming $Q = 10^6$). This timescale is longer than the main-sequence lifetime of an early G-type star, which is expected to be ~10 Gyr; however, this lifetime and $\tau_{\rm circ}$ are on the same order of magnitude. The full picture of evolution from warm to hot Jupiter is not fully understood, and TIC 393818343 b may help complete a picture that suggests tidal migration is more of a spectrum than has previously been understood. Yet despite its sizeable eccentricity, TIC 393818343 b is not eccentric or close enough to its host to migrate inward and become a hot Jupiter under the stated assumptions in a single-planet system.

Tidal circularization might still be possible if tidal dissipation was expedited, but TIC 393818343 b is not well suited for

---

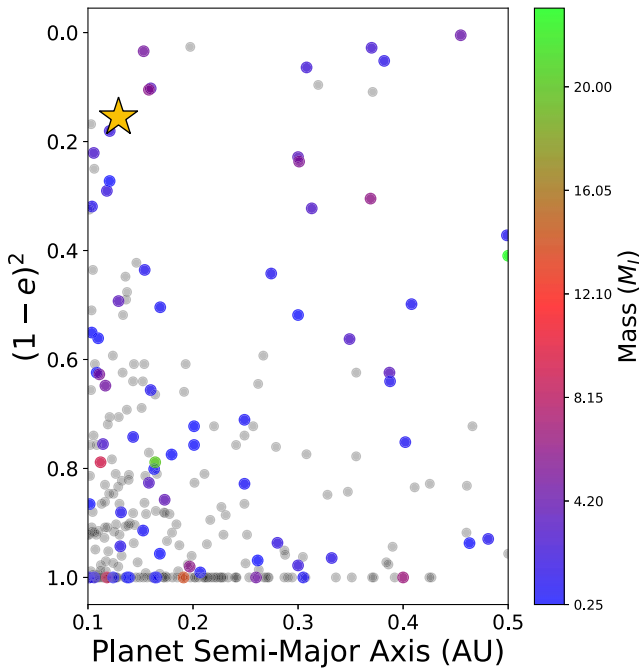[29] Accessed on 2024 May 22 at 07:30 UTC.

Figure 4. Confirmed planets with $10 < P < 200$ days and $0.1 \leqslant a \leqslant 0.5$ au from the NEA that have available mass measurements. Giant planets with $M_P \geqslant 0.25\ M_J$ are plotted such that colors denote the mass of the planet, while planets below this mass cutoff are plotted in gray. The yellow star indicates TIC 393818343 b at $4.34 \pm 0.15\ M_J$.

this scenario. Wu (2018) proposes this enhancement is possible through energy exchange between the orbit and the planet's degree-2 fundamental-mode (f-mode) during periastron passage *if* the planet passes within 4 times the host's tidal radius, $r_\tau = R_P(M_*/M_P)^{1/3}$. Using the methods from Gupta et al. (2023), we calculate a periastron distance $a_{\mathrm{peri}} \approx 7.5\ R_*$. This value is 2.9 times greater than the maximum distance, $4r_\tau = 2.6\ R_*$, at which Wu (2018) states that f-mode dissipation would be effective to boost tidal dissipation efficiency; therefore, TIC 393818343 b's orbit could not be circularized more quickly through this channel.

Considering that only three planets are expected to tidally circularize into hot Jupiters, there is a disconnect between the observed warm and hot Jupiter populations. However, Petrovich & Tremaine (2016) propose a mechanism that can account for much of the hot Jupiter population via secular planet–planet interactions, i.e., in which Kozai-Lidov oscillations occur due to the presence of an outer planetary companion. In this case, warm Jupiters migrate in intervals of high eccentricity but spend more time in low-eccentricity phases and are therefore observed largely at lower eccentricities. As an exercise, we can consider a case in which TIC 393818343 b does circularize via this or some other unknown pathway, despite the values of τ_{circ} and a_{peri}. Again following the analysis of Gupta et al. (2023) and assuming that angular momentum is conserved, the final semimajor axis if TIC 393818343 b were to circularize would be $a_{\mathrm{final}} = 0.0817$ au. Along with the resultant orbital period in this scenario, $P_{\mathrm{final}} = 8.17$ days, this final orbital configuration would land TIC 393818343 b in the hot Jupiter population. Although it is not currently expected to become a hot Jupiter, TIC 393818343 b is an interesting case for further research due to its potential to enter this prolific population if an outer companion is discovered.

Note that the presence of a perturbing outer planet is beyond the scope of this work. Despite no clear evidence from our RV data, the existence of a distant companion cannot be discounted, and we leave this investigation to future studies.

5.2. Opportunities for Atmospheric Characterization

Atmospheric characterization via emission and transmission spectroscopy has become more feasible with the launch of the James Webb Space Telescope (JWST) and other space observatories. To determine the feasibility of follow-up, we can look at the Emission Spectroscopy Metric (ESM) developed by Kempton et al. (2018) based upon the work of Zellem et al. (2017), which is proportional to the S/N that JWST would be expected to achieve with a mid-infrared secondary eclipse detection using MIRI's Low Resolution Spectrometer. Using the properties of TIC 393818343 b derived from this work, including the dayside temperature as $1.10\ T_{\mathrm{eff}}$, the ESM $= 57$, indicating that this planet is a reasonable candidate for emission spectroscopy. Kempton et al. (2018) recommends a threshold of ESM $= 7.5$ for candidates although only terrestrial targets are considered in their analysis for emission spectroscopy.

However, according to the Transmission Spectroscopy Metric (TSM; Zellem et al. 2017; Kempton et al. 2018), TIC 393818343 b is not a suitable target for this type of observation using JWST/NIRISS. For the target, TSM $= 20$, which is lower than the suggested threshold of 96 for sub-Jovians, as TIC 393818343 b is not large or hot enough to be an ideal transmission spectroscopy target.

To compare, Mann et al. (2023) plot various ESM values according to planet mass and temperature for confirmed giant planets ($R > 0.5R_J$) to assess follow-up for the cool giant TOI-2010 b. From their analysis, we can see that TIC 393818343 b's ESM falls among the median for all giant planets as well as those of a similar temperature. Emission spectroscopy of TIC 393818343 b could both expose the temperature structure of its atmosphere via a P-T profile as well as atmospheric abundances, which would add valuable information to the connection between warm and hot Jupiters (Madhusudhan 2019; Fortney et al. 2021). Chemical composition and abundances may indicate whether a gas giant formed in situ or migrated inwards, a key question in the general formation of warm Jupiters and, although emission spectra are available for many hot Jupiters, there is a paucity of this data for their cooler cousins.

Considering the ESM and an extremely likely occultation of TIC 393818343 b ($b_s = 0.123\ ^{+0.11}_{-0.086}$; see Equation (7) of Winn et al. 2010), we believe it is a suitable candidate for emission spectroscopy follow-up. Secondary eclipse timing, T_S, is available in Table 3. Note that, due to its small semimajor axis a, TIC 393818343 b is not a reasonable target for direct imaging observations.

6. Summary

Here we present a confirmation of the TESS-discovered exoplanet TIC 393818343 b. First identified as a candidate from a single TESS transit in Sector 55, we gathered follow-up RV and photometric observations using both the APF at Lick Observatory and a network of citizen scientists. Our analyses show that TIC 393818343 b is a warm Jupiter, with $P = 16.25$ days and $a = 0.1291$ au, on a highly eccentric orbit, $e = 0.6058$, around an early G-type star. Its orbital parameters indicate that,

if the orbit were to circularize, TIC 393818343 b would join the hot Jupiter population; however, the timescale for which this would take place via the tidal migration pathway is longer than the main-sequence lifetime of the host star.

We note that this planet is a candidate for atmospheric characterization via emission spectroscopy although it is not a feasible target for transmission spectroscopy or direct imaging. Future studies of TIC 393818343 b's atmosphere with space telescopes such as JWST or the Hubble Space Telescope could add to the ongoing investigation as the scientific community continues to characterize the warm Jupiter population.

The crucial data from ground-based observations to confirm the planetary nature of TIC 393818343 b demonstrate the impact of the burgeoning field of citizen science. These data constrained the orbital parameters modeled with EXOFASTv2 and confirmed the period derived from the RV analysis. Due to the global nature of the Unistellar Network and Exoplanet Watch, weather effects were mitigated, and multiple observations were possible during each campaign, furthering the significance of our detections. This discovery adds to the multiple publications over various fields resulting from such citizen science observations, e.g., Zellem et al. (2020), Pearson et al. (2022), Perrocheau et al. (2022), Graykowski et al. (2023), Sgro et al. (2023), and Peluso et al. (2024). These networks of amateur and professional astronomers will continue to be vital in keeping ephemerides fresh for TIC 393818343 b and other confirmed exoplanets, as well as in the confirmation of future candidates.

ORCID iDs

Lauren A. Sgro ⓘ https://orcid.org/0000-0001-6629-5399
Paul A. Dalba ⓘ https://orcid.org/0000-0002-4297-5506
Thomas M. Esposito ⓘ https://orcid.org/0000-0002-0792-3719
Franck Marchis ⓘ https://orcid.org/0000-0001-7016-7277
Diana Dragomir ⓘ https://orcid.org/0000-0003-2313-467X
Steven Villanueva, Jr. ⓘ https://orcid.org/0000-0001-6213-8804
Benjamin Fulton ⓘ https://orcid.org/0000-0003-3504-5316
Mario Billiani ⓘ https://orcid.org/0000-0002-3278-9590
Margaret Loose ⓘ https://orcid.org/0000-0002-5215-4779
Nicola Meneghelli ⓘ https://orcid.org/0000-0002-5105-635X
Darren Rivett ⓘ https://orcid.org/0000-0002-1240-6580
Fadi Saibi ⓘ https://orcid.org/0009-0003-6483-0433
Sophie Saibi ⓘ https://orcid.org/0009-0006-8494-5408
Bryan Martin ⓘ https://orcid.org/0009-0005-2850-1098
Georgios Lekkas ⓘ https://orcid.org/0000-0003-3559-0840
Robert T. Zellem ⓘ https://orcid.org/0000-0001-7547-0398
Ivan A. Terentev ⓘ https://orcid.org/0000-0002-0654-4442
Robert Gagliano ⓘ https://orcid.org/0000-0002-5665-1879
Thomas Lee Jacobs ⓘ https://orcid.org/0000-0003-3988-3245
Martti H. Kristiansen ⓘ https://orcid.org/0000-0002-2607-138X
Daryll M. LaCourse ⓘ https://orcid.org/0000-0002-8527-2114
Hans M. Schwengeler ⓘ https://orcid.org/0000-0002-1637-2189

References

Adams, F. C., & Laughlin, G. 2006, ApJ, 649, 1004

Astropy Collaboration, Price-Whelan, A. M., Sipőcz, B. M., et al. 2018, AJ, 156, 123

Astropy Collaboration, Robitaille, T. P., & Tollerud, E. J. 2013, A&A, 558, A33

Bailer-Jones, C. A. L., Rybizki, J., Fouesneau, M., Mantelet, G., & Andrae, R. 2018, AJ, 156, 58

Baruteau, C., Crida, A., Paardekooper, S.-J., et al. 2014, in Protostars and Planets VI, ed. H. Beuther et al. (Tucson, AZ: Univ. of Arizona Press), 667

Butler, R. P., Marcy, G. W., Williams, E., et al. 1996, PASP, 108, 500

Chatterjee, S., Ford, E. B., Matsumura, S., & Rasio, F. A. 2008, ApJ, 686, 580

Conzo, G., & Moriconi, M. 2024, RNAAS, 8, 53

Cutri, R. M., Skrutskie, M. F., van Dyk, S., et al. 2003, yCat, II/246

Cutri, R. M., Wright, E. L., Conrow, T., et al. 2014, yCat, II/328

Dalba, P. A., & Muirhead, P. S. 2016, ApJL, 826, L7

Dalba, P. A., Muirhead, P. S., Croll, B., & Kempton, E. M.-R. 2017, AJ, 153, 59

Dawson, R. I., & Johnson, J. A. 2018, ARA&A, 56, 175

Dong, J., Huang, C. X., Dawson, R. I., et al. 2021, ApJS, 255, 6

Dotter, A. 2016, ApJS, 222, 8

Eastman, J. 2017, EXOFASTv2: Generalized publication-quality exoplanet modeling code, v2, Astrophysics Source Code Library, ascl:1710.003

Eastman, J., Gaudi, B. S., & Agol, E. 2013, PASP, 125, 83

Eastman, J. D., Rodriguez, J. E., Agol, E., et al. 2019, arXiv:1907.09480

Ford, E. B., & Rasio, F. A. 2006, ApJL, 638, L45

Fortney, J. J., Dawson, R. I., & Komacek, T. D. 2021, JGRE, 126, e2020JE006629

Fulton, B. J., Weiss, L. M., Sinukoff, E., et al. 2015, ApJ, 805, 175

Gaia Collaboration, Brown, A. G. A., Vallenari, A., et al. 2018, A&A, 616, A1

Gaia Collaboration, Prusti, T., de Bruijne, J. H. J., et al. 2016, A&A, 595, A1

Gelman, A., & Rubin, D. B. 1992, StaSc, 7, 457

Goldreich, P., & Tremaine, S. 1980, ApJ, 241, 425

Graykowski, A., Lambert, R. A., Marchis, F., et al. 2023, Natur, 616, 461

Gupta, A. F., Jackson, J. M., Hébrard, G., et al. 2023, AJ, 165, 234

Gupta, A. F., Millholland, S. C., Haedam, I., et al. 2024, Natur, in press

Hall, C., Dong, R., Teague, R., et al. 2020, ApJ, 904, 148

Jenkins, J. M., Twicken, J. D., McCauliff, S., et al. 2016, Proc. SPIE, 9913, 99133E

Kass, R. E., & Raftery, A. E. 1995, JASA, 90, 773

Kempton, E. M. R., Bean, J. L., Louie, D. R., et al. 2018, PASP, 130, 114401

Kokori, A., Tsiaras, A., Edwards, B., et al. 2022, ApJS, 258, 40

Kokori, A., Tsiaras, A., Edwards, B., et al. 2023, ApJS, 265, 4

Kozai, Y. 1962, AJ, 67, 591

Kristiansen, M. H., Rappaport, S. A., Vanderburg, A. M., et al. 2022, PASP, 134, 074401

Lidov, M. L. 1962, P&SS, 9, 719

Lightkurve Collaboration, Cardoso, J. V. d., Hedges, C., et al. 2018, Lightkurve: Kepler and TESS time series analysis in Python, 1.11, Astrophysics Source Code Library. ascl:1812.013

Lindegren, L., Klioner, S. A., Hernández, J., et al. 2021, A&A, 649, A2

Madhusudhan, N. 2019, ARA&A, 57, 617

Mann, C. R., Dalba, P. A., Lafrenière, D., et al. 2023, AJ, 166, 239

Marchis, F., Malvache, A., Marfisi, L., Borot, A., & Arbouch, E. 2020, AcAau, 166, 23

MAST Team 2021, TESS Light Curves - All Sectors, STScI/MAST doi:10.17909/T9-NMC8-F686

Mayor, M., & Queloz, D. 1995, Natur, 378, 355

Naef, D., Latham, D. W., Mayor, M., et al. 2001, A&A, 375, L27

Nagasawa, M., Ida, S., & Bessho, T. 2008, ApJ, 678, 498

Naoz, S. 2016, ARA&A, 54, 441

NASA Exoplanet Archive 2024, Planetary Systems, Version: 2024-05-22 20:00, NExScI-Caltech/IPAC doi:10.26133/NEA12

NExScI 2022, Exoplanet Follow-up Observing Program Web Service, IPAC doi:10.26134/EXOFOP5

Paneque-Carreño, T., Pérez, L. M., Benisty, M., et al. 2021, ApJ, 914, 88

Pearson, K. A., Beichman, C., Fulton, B. J., et al. 2022, AJ, 164, 178

Peluso, D. O., Dalba, P. A., Wright, D., et al. 2024, AJ, 167, 170

Peluso, D. O., Esposito, T. M., Marchis, F., et al. 2023, PASP, 135, 015001

Perrocheau, A., Esposito, T. M., Dalba, P. A., et al. 2022, ApJL, 940, L39

Petigura, E. A. 2015, PhD thesis, University of California, Berkeley

Petigura, E. A., Howard, A. W., Marcy, G. W., et al. 2017, AJ, 154, 107

Petrovich, C., & Tremaine, S. 2016, ApJ, 829, 132

Radovan, M. V., Cabak, G. F., Laiterman, L. H., Lockwood, C. T., & Vogt, S. S. 2010, Proc. SPIE, 7735, 77354K

Radovan, M. V., Lanclos, K., Holden, B. P., et al. 2014, Proc. SPIE, 9145, 91452B

Rafikov, R. R. 2006, ApJ, 648, 666

Rasio, F. A., & Ford, E. B. 1996, Science, 274, 954

Ricker, G. R., Winn, J. N., Vanderspek, R., et al. 2015, JATIS, 1, 014003

Schlafly, E. F., & Finkbeiner, D. P. 2011, ApJ, 737, 103

Schmitt, A., & Vanderburg, A. 2021, arXiv:2103.10285

Schmitt, A. R., Hartman, J. D., & Kipping, D. M. 2019, arXiv:1910.08034

Sgro, L. A., Esposito, T. M., Blaclard, G., et al. 2023, RNAAS, 7, 141

Vallenari, A., Brown, A. G. A., Prusti, T., et al. 2023, A&A, 674, A1

Vogt, S. S., Allen, S. L., Bigelow, B. C., et al. 1994, Proc. SPIE, 2198, 362

Vogt, S. S., Radovan, M., Kibrick, R., et al. 2014, PASP, 126, 359

Winn, J. N., Fabrycky, D., Albrecht, S., & Johnson, J. A. 2010, ApJL, 718, L145

Wu, Y. 2018, AJ, 155, 118

Wu, Y., & Lithwick, Y. 2011, ApJ, 735, 109

Wu, Y., & Murray, N. 2003, ApJ, 589, 605

Zellem, R. T., Pearson, K. A., Blaser, E., et al. 2020, PASP, 132, 054401

Zellem, R. T., Swain, M. R., Roudier, G., et al. 2017, ApJ, 844, 27